Electro-optic camera system for measurement of the underwater radiance distribution

Kenneth J. Voss, MEMBER SPIE
University of California, San Diego
Scripps Institution of Oceanography
Institute of Marine Resources
La Jolla, California 92093-0218

Abstract. A new instrument for measuring the underwater spectral radiance distribution is described. This instrument, the electro-optic radiance distribution camera system (RADS), is based on two electro-optic charge-injection device cameras with fisheye lenses and a filter changer for selection of the spectral region of interest. RADS allows a complete spectral radiance distribution to be measured in a short period of time and allows routine reduction to absolute radiometric data. Many other apparent optical properties such as vector irradiance, scalar irradiance, average cosine, and net irradiance can be derived from these radiance data. In this paper, the instrument is described, values of other optical properties derived from the data are presented, and the inherent optical property of absorption is calculated from the radiance distributions using Gershun's law.

Subject terms: ocean optics; radiance distribution.

Optical Engineering 28(3), 241-247 (March 1989).

CONTENTS

1. INTRODUCTION

The underwater radiance distribution contains the most complete set of apparent optical parameters (those parameters that depend on the geometrical structure of the light field[1]) that one can measure. Because of the completeness of the measurement, not only can the radiance distribution be used to obtain scalar irradiance, vector irradiance, and apparent optical properties such as the diffuse attenuation coefficient and reflectance, but it is also theoretically possible to derive the inherent optical properties (those parameters that are independent of the geometrical structure of the light field[1]) of volume scattering function and absorption coefficient from the variation of the radiance distribution with depth. In the past it has been difficult and time consuming to measure the radiance distribution and to perform the subsequent analysis, and therefore few measurements have been obtained.

A new instrument for measuring the underwater spectral radiance distribution, the electro-optic radiance distribution camera system (RADS), allows a complete spectral radiance distribution to be measured in a short period of time and allows routine reduction of these data to absolute radiometric values. In this paper, the instrument and the calibration techniques used in the reduction of data are described. Sample data, taken in the coastal waters off San Diego, are shown, along with examples of optical properties derived from these data.

2. RADIANCE DISTRIBUTION THEORY

Radiance is defined as the radiant flux per unit solid angle per unit projected area from a given direction.[2] The spectral radiance distribution is the collection of radiance data for all directions at a given point in space at a certain wavelength.

Paper 2537 received Feb. 26, 1988; revised manuscript received Dec. 2, 1988; accepted for publication Dec. 2, 1988.

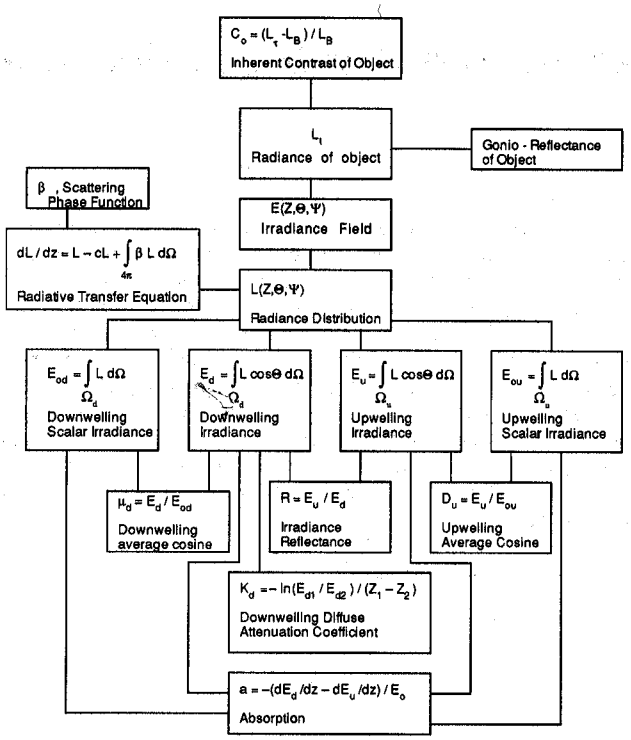

Fig. 1. Chart of inherent and apparent optical properties and their relationship to the radiance distribution.[5]

For even one wavelength, the spectral radiance distribution contains an enormous amount of data, so at a resolution of 1° (or 1 msr), it contains more than 13,000 discrete values. All apparent optical properties can be derived from a collection of radiance distribution measurements. Figure 1 illustrates how the radiance distribution fits into the overall scheme of hydrologic optical properties. The downwelling scalar irradiance E_{od} is simply the integral of the radiance distribution over solid angle, or

$$E_{od} = \int_{\Omega_d} L\, d\Omega \,, \tag{1}$$

where Ω_d is the portion of the solid angle with zenith angles less than 90° and L is the radiance distribution. The more commonly measured downwelling irradiance E_d is the cosine-weighted integral of the radiance distribution over solid angle, or

$$E_d = \int_{\Omega_d} L \cos\theta\, d\Omega \,, \tag{2}$$

where θ is the zenith angle. The average cosines are obtained, once the vector and scalar irradiances have been derived, by

$$\mu_d = \frac{E_d}{E_{od}} = \frac{\int_{\Omega_d} L \cos\theta\, d\Omega}{\int_{\Omega_d} L\, d\Omega} \,. \tag{3}$$

If the radiance distribution is known for two different depths, assuming negligible change in the incident light field between these measurements, the average diffuse attenuation coefficients can be derived in the standard manner from the irradiances once they are obtained as above.

The inherent optical property of absorption, a, can theoretically be obtained, under the same restrictions as above, using Gershun's law[3]:

$$a = -\frac{1}{E_o}\frac{dE}{dz} \,, \tag{4}$$

where E is the net vector irradiance ($E_d - E_u$) [E_u is the upwelling irradiance], z is the depth, and E_o is the total scalar irradiance ($E_{ou} + E_{od}$). If one approximates the decrease of E for short depth increments as following Beer's law, then E can be represented by

$$E(z) = E \exp(-K_E z) \,, \tag{5}$$

where K_E is the vector irradiance attenuation coefficient, and Gershun's law takes the form

$$a = \frac{K_E E}{E_o} \,. \tag{6}$$

The scattering phase function $\beta(\Psi)$[Ψ is the angle through which the light is scattered], another inherent property of seawater, can theoretically be obtained by inversion of the radiative transfer equation. For example, Zaneveld[4] outlined a procedure to obtain the phase function by inverting an axially symmetric radiance distribution. This method involves decomposing the radiance distribution into Legendre functions (P_n) so that

$$\beta(\Psi) = \sum \frac{(2n+1)}{4\pi} P_n(\cos\Psi) \times \left[c + \frac{\int (dL/dz) P_n(\cos\theta) \cos\theta \sin\theta\, d\theta}{\int L P_n(\cos\theta) \sin\theta\, d\theta} \right] , \tag{7}$$

where c is the beam attenuation coefficient.

In addition to these apparent and inherent optical properties, several other problems in optical oceanography requiring knowledge of the radiance distribution can be solved. As an example, the inherent contrast of an object can be predicted using the radiance distribution and the gonio-reflectance of the object.[5] Once the inherent contrast of the object is determined, the apparent contrast can be determined using the diffuse attenuation coefficient K and the beam attenuation coefficient c, both derivable from the radiance distribution measurements. As one can see, the radiance distribution is a basic measurement of ocean optical properties.

3. PAST MEASUREMENT TECHNIQUES

The radiance distribution has not been the measurement of choice in optical oceanography owing to the volume of data that must be collected and the difficulty with which it has been collected. The initial method used to collect radiance distribu-

tion information was to make individual measurements with a Gershun tube radiometer (e.g., see Tyler[6]). The problem with making measurements in this manner is that the radiance distribution is dependent on the incident radiance field and therefore must be measured in a short time, relative to changes in the incident light field. Even if measurements are taken at only 10° intervals of zenith and azimuth angle, more than 600 measurements must be obtained. Many later studies[7] were restricted to just one plane of measurement (usually in the zenith plane of the sun) and do not allow many of the other optical parameters to be derived.

The next advance in measurement techniques, described by Smith et al.,[5] involved the use of two photographic cameras with fisheye camera lenses. A fisheye lens characteristically projects a hemisphere of radiance information onto the film plane; therefore, with the two cameras the full 4π radiance distribution is measured in the two images. This method allowed rapid data acquisition in a format well suited to handling the large volume of data required. The failure of this method lies in the use of photographic cameras to obtain the radiometric information and the limited spectral filtering used. Photographic radiometry is difficult and time consuming to perform and generally of poor precision.

The method we have chosen is similar to that of Smith et al.[5] but involves the use of electro-optic charge-injection device (CID) cameras. This method thus has the advantages of the photographic method (use of imagery to store and process the data) but avoids the pitfalls of photographic radiometry.

4. INSTRUMENT DESIGN

Figure 2 is a stylized block diagram of the instrument. Two GE-2509 CID cameras are used to collect the underwater radiometric data, with a Poynting 509 frame grabber and digitizer to transform the data into a digital signal. This signal is sent up the multiconductor cable to the shipboard computer to be displayed, in false color imagery, and stored on disk or tape.

4.1. Optical instrumentation

A fisheye converter lens (Bicar) is used as the input to the optical train. Conventionally, this lens is used in conjunction with a lens of normal focal length to provide a wide-angle or "fisheye" field of view. In our application, however, it is used as the input to the series of lenses in the filter changer optics. The fisheye lens system characteristically projects a 2π sr hemisphere onto the film plane via an equidistant projection.[9] In equidistant projection the zenith angle θ is projected onto the film plane through the equation

$$r = f\theta \,, \tag{8}$$

where f is the effective focal length of the lens system and r is the radial distance from the center on the image plane. For an ideal lens following this type of projection, the solid angle $d\Omega$ can be shown[9] to be related to the area on the image plane dS by the equation

$$d\Omega = \frac{1}{f^2}\frac{\sin\theta}{\theta}\,dS \,. \tag{9}$$

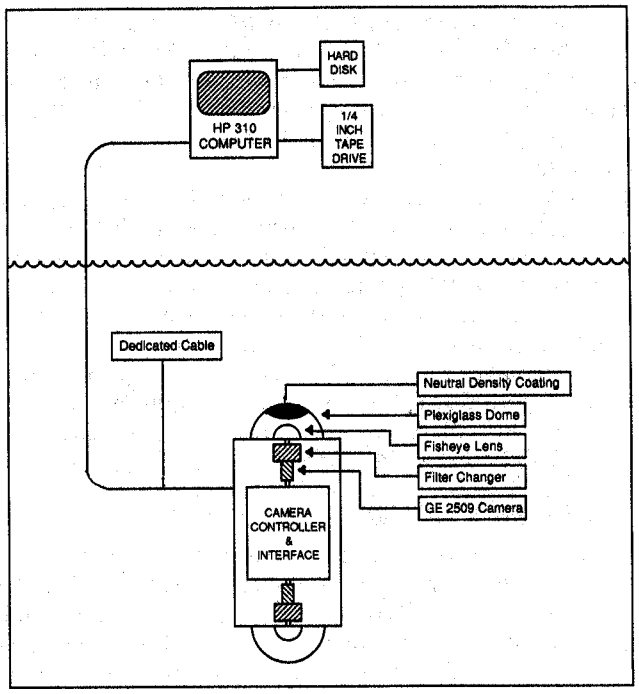

Fig. 2. Schematic of RADS electro-optic radiance distribution camera system.[8]

The filter changer was designed to be inserted between the fisheye lens and the camera to determine the camera system's spectral response. The filter changer allows four spectral filters (interference filters with approximate bandpass of 25 nm and centers at 450, 500, 550, and 600 nm) and four absorption neutral density filters (to adjust the overall scene dynamic range to the optimum camera level) to be inserted into the optical path. The light is not collimated at the points where the spectral and neutral density filters are inserted; however, the maximum deviation of a light ray from the normal to the optical train is only 16°. This small angle causes a negligible shift in the center and bandwidth of the spectral filter. The filter changer is controlled from the ocean surface, allowing measurement of multiple spectral ranges during a single hydrocast. The resultant optical system allows measurement of the radiance distribution from 0° zenith to 87.5° zenith for the downwelling radiance distribution and from 92.5° to 180° for the upwelling radiance distribution.

Plastic hemispherical domes are used as windows in this instrument. For the downwelling radiance distribution window, a neutral density coating (one optical density) was applied in the region between 0° and 48° zenith angle. This region of the downwelling distribution is assumed to be the brightest area in the underwater images ("manhole" effect[1]) since all skylight is refracted into this angular range by the air-water interface. The neutral density coating increases the effective intrascene dynamic range of the camera to more than 3 orders of magnitude.

The heart of RADS is the two GE-2509 CID cameras. These cameras are 260×253 pixel cameras with low blooming and, as described later, an intrascene dynamic range of over 2 logs. These cameras allow on-chip integration to occur during frame periods through the use of injection inhibit. In this

process the camera is not cleared between frame periods (the process of clearing is called injection),[10] thus allowing the pixel array to accumulate charge over several frame increments and thus allowing low light level images to be collected. This extends the maximum depth to which the camera system can operate.

To measure the surface incoming radiation, a separate camera system is placed on deck in an active stable table. This system consists of another GE-2509 camera, filter changer system, Poynting 509 camera controller (with a parallel computer interface versus the serial interface used in the underwater system), and an occulter to reduce the radiance from the sun to a manageable level. The measurement of incoming radiance distribution can be used both as input to a radiative transfer model and to test for variations of incident flux during the underwater measurement.

4.2. Data track

A Poynting 509 frame grabber converts the images to 8 bit digital data. The frame grabber was repackaged and inserted into the underwater unit so that the analog video signal could be digitized at the source (camera), thus minimizing signal degradation. An RS-232, 9600-baud link is used between the frame grabber and the surface computer, and all video data are transferred up this digital link.

A Hewlett Packard 310C microcomputer is used for overall instrument control and data manipulation. The data are entered into this computer in byte form from the RS-232 data link and are stored on a hard disk during data collection. For permanent archiving a Hewlett Packard 9144A ¼ in. cartridge tape drive is used, which has the capacity to store 182 Mbytes of data per cartridge. The color CRT allows data to be displayed on screen as false color images, or images can be sent to the surface camera controller and displayed in gray scale tones on a video monitor.

A complete data package consists of two underwater images (one up and one down) and two surface images, one taken before each underwater image. This amounts to approximately 262 kbytes of data per depth and wavelength, which necessitates careful planning of both data storage and data reduction techniques. The first step in data reduction is subtraction of a dark field image from the data image. This eliminates the pixel-dependent, time-independent portion of the dark current. Conversion of the subtracted data to logarithmic flux levels, using an experimentally determined linearity function, is then performed. The actual time-dependent image dark current is determined by sampling a region of the CID array that is outside the area of the lens projection. The average value of a 5×5 square area of the array is used as an indication of this thermally generated dark noise in the data array, and this value is subtracted from each pixel in the image. The image is then multiplied by a calibration number that includes factors dealing with the absolute calibration, number of frame periods averaged (using the on-chip injection inhibit function), and the filter changer neutral density. Finally, the downwelling radiance image is multiplied by an image that inverts the effects of the neutral density coating in the center of the window dome. This entire data reduction process takes approximately 4 min per image (on the HP 310C) and is arranged so that batch processing can take place, allowing as much as 45 images to be reduced without operator intervention (limited only by the 10 Mbyte hard disk capacity).

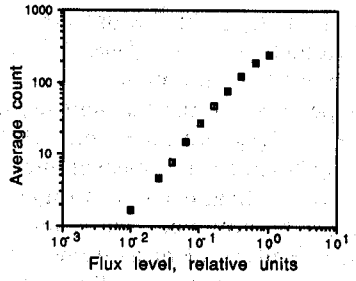

Fig. 3. Example of a typical linearity calibration for the electro-optic cameras.

5. CALIBRATION

The calibration procedures are detailed elsewhere,[11] but a brief description of the procedures are presented.

5.1. Linearity calibration

Figure 3 shows the results of the linearity calibration on one of the cameras. The linearity of the response is a function of both the camera and the frame digitizer; therefore, the calibration is performed on each camera independently. The camera-digitizer systems were found to be linear over a range of flux of 1.8 logs, with well-behaved behavior to beyond 2.4 logs. This procedure was performed in the following manner: The camera was placed, without optics, behind a diffusing plate to enable unfocused light to flood the array. A lamp, on the other side of the diffusing plate, was placed at various distances from the diffusing plate. The relative irradiance on the camera array was thus determined by the inverse square of the distance from the lamp to the diffusing plastic. The curve resulting from the linearity test was fitted in three segments by a linear relation in each segment.

5.2. Absolute calibration

An absolute calibration was performed on the system using standard radiometric techniques. A 1000 W lamp (Optronic Laboratories, Inc., model FEL-C), with known irradiance characteristics traceable to the National Bureau of Standards, was used to irradiate a reflectance plaque (coated with barium sulfate paint, Eastman Kodak), creating a source of known radiance. The fields of view of the cameras were individually centered on this plaque and an image was obtained. The linearity curves obtained from the linearity calibration were applied to the image, and a calibration factor was obtained from the portion of the image viewing the plaque. During the linearity calibration, different areas of the image were averaged and found to have the same response to within one count, implying relatively uniform sensitivity; therefore, the same calibration factor, determined for the central portion of the array, was applied to the whole image.

5.3. Angular calibration

Angular calibration was performed by centering each camera in a large hemispherical dome and placing a light source at known angles with respect to the camera. Images were taken with the camera, and the center of the light source was determined in the image. The pixel locations of the light source were converted to pixel radius values from the center of the image, and a least square fit of pixel radius versus zenith angle

Fig. 4. Example of a calibrated downwelling radiance distribution image taken from the ship R/V Sproul on April 15, 1987, during a cruise off the San Diego coast. The image was taken at 10 m depth, 9:00 PDT, and the spectral filter was 450 nm. The image is displayed in contours such that each gray scale step is 0.25 log, with an overlapping of gray scales every full log. Brightest part of the image is between $10^{1.5}$ and $10^{1.75}$ $\mu W \cdot sr^{-1} \cdot nm^{-1} \cdot cm^{-2}$; lowest values are between $10^{-1.75}$ and $10^{-2.00}$ $\mu W \cdot sr^{-1} \cdot nm^{-1} \cdot cm^{-2}$.

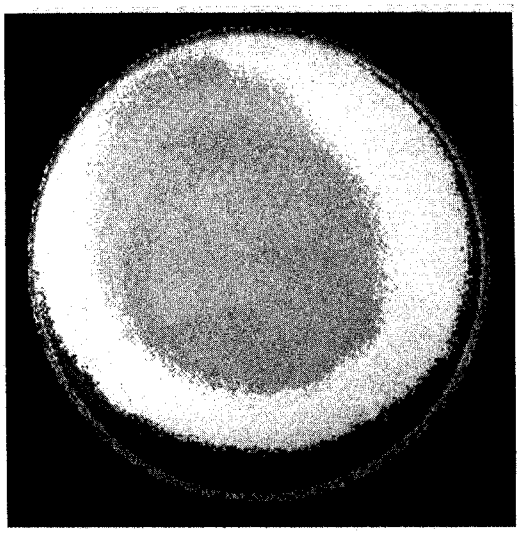

Fig. 5. Example of a calibrated upwelling radiance distribution image; same depth, time, location, and spectral range as Fig. 4. Brightest part of the image is between 10^{-1} and $10^{-0.75}$ $\mu W \cdot sr^{-1} \cdot nm^{-1} \cdot cm^{-2}$ (on the edge of the image); lowest values are between $10^{-2.75}$ and $10^{-2.50}$ $\mu W \cdot sr^{-1} \cdot nm^{-1} \cdot cm^{-2}$ (center of the image).

was performed. In this manner the f value (effective focal length of the lens system) in Eq. (8) was determined.

The angular response of the system was measured and found to follow the above ideal response [Eqs. (8) and (9)] quite well. There was, however, an additional rolloff R of the lens, which was fit by the equation

$$R = \cos^{0.231}\theta \ . \tag{10}$$

At present, the accuracy of the instrument is 12%, with a precision of approximately 5%. An experiment was performed in which the deck camera, which measures the incident radiation at the sea surface, was compared with a standard sky radiometer, and very good agreement was obtained between these two instruments.[11]

6. EXAMPLE DATA

6.1. Image data

Figure 4 is an example of a calibrated downwelling radiance distribution image. Obvious in this image are the effect of the ship shadow (the large shadowing in the upper right) and the shadowing due to the cable (lower left corner). Techniques are currently being developed to investigate ways of reducing, or correcting, these shadowing effects. The black ring in the image is the area where the data were judged to be suspect and therefore were excluded. This ring falls on the edge of the neutral density coating used to reduce the intensity in the center of the image, and a slight defocusing caused by the variations in filter glass thickness caused a blurring of this edge. At 10 m depth the direct solar beam still is a large component of the downwelling radiance field, and the whole radiance field is skewed toward the refracted solar beam.

Figure 5 shows the upwelling radiance distribution from the same time and depth as the downwelling radiance distribution of Fig. 4. As expected, this image shows much less variation than the downwelling radiance distribution, illustrating the flatness of the upwelling radiance distribution. The ship shadow appears to be affecting the upwelling image in that the upwelling radiance is skewed and not symmetric around the nadir. The lowest radiance region of the image appears to extend from the center of the image toward the area beneath the ship at an azimutal angle of 180° to the direct solar component.

6.2. Derived properties

To illustrate the use of the radiance distribution to obtain other optical properties, we chose the two pairs of images shown in Fig. 6. Figure 7 is a graph of the beam transmittance at 490 nm as measured by the Vislab spectral transmissometer (VLST) at the same station as Fig. 6, which illustrates that the optical properties of the water column were changing over the depths at which the radiance distribution was measured.

The values of downwelling irradiance (E_d), upwelling irradiance (E_u), downwelling scalar irradiance (E_{od}), and upwelling scalar irradiance (E_{ou}) were calculated from these images and are shown in Table I. We call these properties first level derived products since they are calculated directly from each 2π radiance distribution and do not depend on stability of the ambient light field.

Table II illustrates the second level of derived products. Calculation of R_{scalar} (E_{ou}/E_{od}), R_{vector} (E_u/E_d), μ_d, and μ_u depends on the stability of the incident light field during the measurement process and the time it takes to make both the upwelling and downwelling radiance distribution measurements. The stability of the incident light field can be determined using data from the deck camera.

The products in the third level depend on the incident light field's staying constant over a time frame of two data packages, or about 10 min. The light field was found to be sufficiently constant for these images, and therefore the values of the diffuse attenuation coefficient K and absorption coefficient a were calculated from the image data; these values are

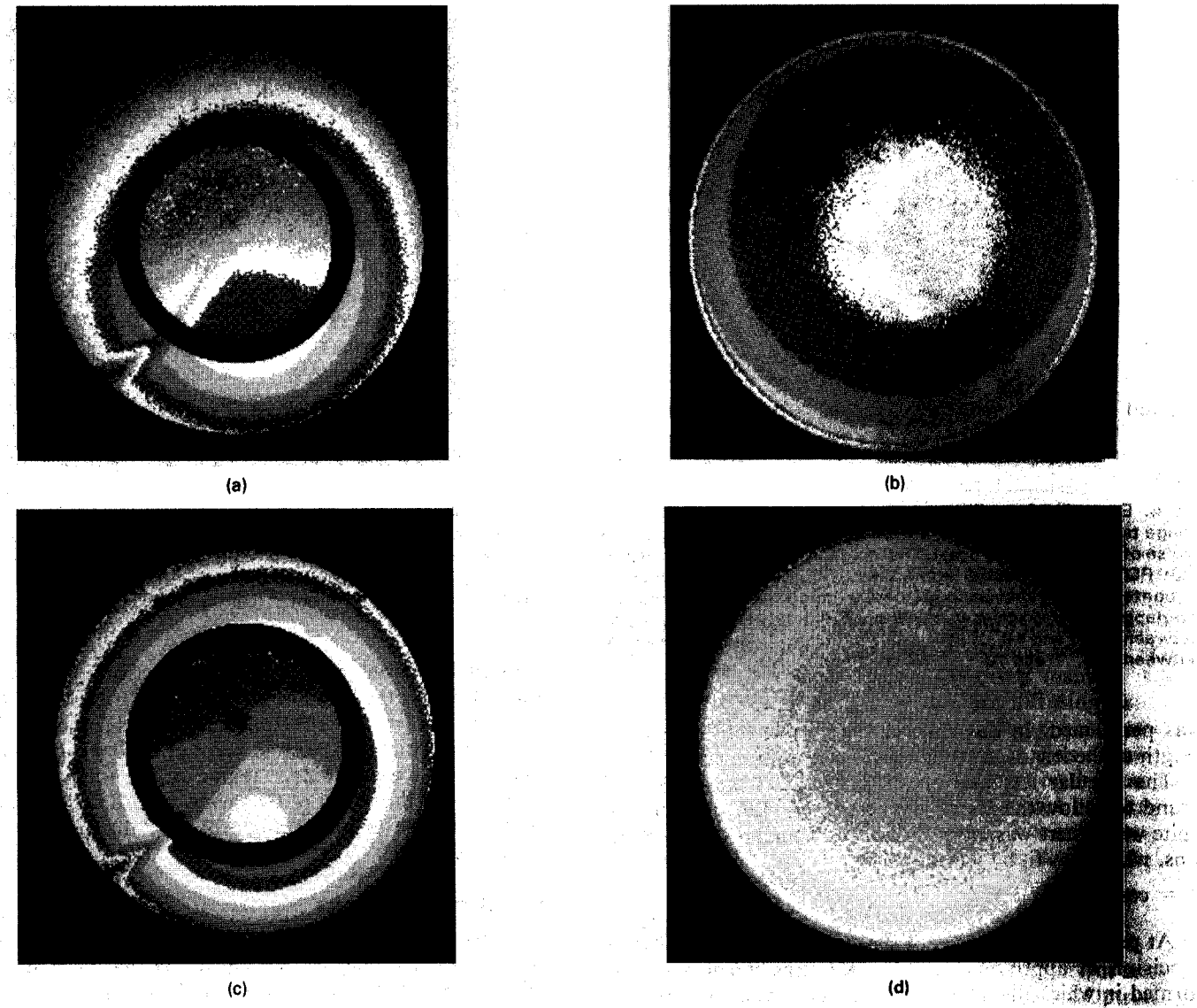

Fig. 6. Images used for calculation of other apparent optical properties, all taken on April 14, 1987, off the San Diego coast at approximately 15:00 PDT, measured at 500 nm. (a) Downwelling and (b) upwelling radiance distribution at 40 m. (c) Downwelling and (d) upwelling radiance distribution at 60 m.

shown in Table III. A value for the total scattering coefficient b was determined using the approximate relationship

$$K = a + \frac{b}{6} \cdot \tag{11}$$

When the value of b derived as above is added to the value of a calculated from Gershun's law,[3] a value for the beam attenuation coefficient c is obtained. The value obtained in this manner is compared with the directly measured value for c in Table III.

7. CONCLUSION

A new instrument for measuring the radiance distribution in the ocean has been described. This electro-optic radiance distribution camera system is a valuable tool for investigating the apparent optical properties of the upper ocean. Data taken with this instrument have been presented, and some of the theoretical relationships linking the apparent optical properties with the inherent optical properties have been illustrated.

At present, these data are also being used to test radiative transfer models, which predict the radiance distribution and other apparent optical properties, and to look at the air-sea interface, clouds, and other factors that affect the incident radiation field and therefore the apparent optical properties.

8. ACKNOWLEDGMENTS

This research was supported by the Office of Naval Research, contract No. N00014-85C-0730. I would like to thank Roswell Austin for his support and ideas and acknowledge the contributions of Richard Johnson in the filter changer ideas and construction. I would also like to thank Harry Sprink and Albert Chapin for their technical support, J. C. Brown for his graphical support, and Charles Trees for his review of the manuscript.

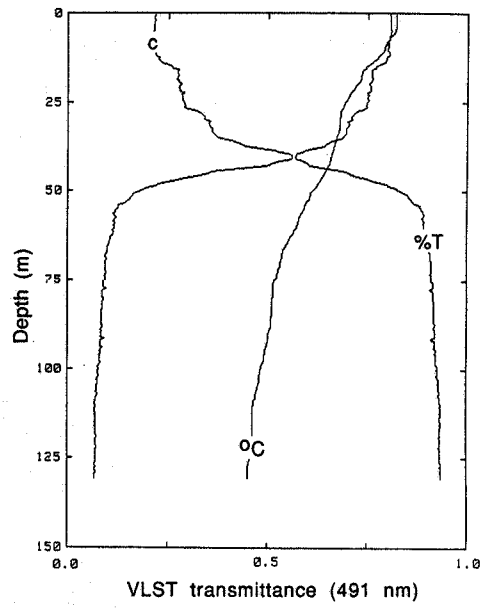

Fig. 7. Beam transmittance at 490 nm as measured by the Vislab spectral transmissometer, at the same station as the images of Fig. 6. Volume attenuation coefficient (c) range: 0 to 1. Temperature (°C) range: 0 to 20°C.

9. REFERENCES

1. R. W. Preisendorfer, *Hydrologic Optics, Vol. 1,* U.S. Dept. of Commerce, Nat'l. Oceanographic and Atmospheric Admin., Environmental Research Lab., Honolulu, Hawaii (1976).
2. A. Morel and R. C. Smith, "Terminology and units in optical oceanography," Marine Geodesy 5, 335–349 (1982).
3. A. Gershun, "The light field," J. Math. Phys. 18, 51–151 (1939).
4. J. R. V. Zaneveld, "New developments of the theory of radiative transfer in the oceans," in *Optical Aspects of Oceanography,* N. G. Jerlov and E. Steemen Nielsen, eds., pp. 121–134, Academic Press, New York (1974).
5. R. C. Smith, R. W. Austin, and J. E. Tyler, "An oceanographic radiance distribution camera system," Appl. Opt. 9, 2015–2022 (1970).
6. J. E. Tyler, "Radiance distribution as a function of depth in an underwater environment," in *Light in the Sea,* J. E. Tyler, ed., pp. 233–252, Dowden, Hutchinson & Ross, Inc., Stroudsburg, Pa. (1977).
7. T. Sasaki, "On the instruments for measuring angular distributions of underwater daylight intensity," in *Light in the Sea,* J. E. Tyler, ed., pp. 190–195, Dowden, Hutchinson & Ross, Inc., Stroudsburg, Pa. (1977).
8. K. J. Voss, "Radiance distribution measurements in coastal water," in *Ocean Optics IX,* M. A. Blizard, ed., Proc. SPIE 925, 56–66 (1988).
9. K. Miyamoto, "Fish-eye lens," J. Opt. Soc. Am. 54, 1016–1061 (1964).
10. G. R. Sims and M. B. Denton, "Characterization of a charge-injection-device camera system as a multichannel spectroscopic detector," Opt. Eng. 26(10), 1008–1019 (1987).
11. K. J. Voss and G. Zibordi, "Radiometric and geometric calibration of a visible spectral electro-optic 'fisheye' camera radiance distribution system," J. Atmos. Ocean. Tech., in press (1989).

TABLE I. First level derived products, irradiance values. (These values were derived from the images in Fig. 6. Units are $\mu W \cdot cm^{-2} \cdot nm^{-1}$.)

	40 m	60 m
E_d	0.601	0.256
E_u	0.0210	0.0054
E_{od}	0.808	0.325
E_{ou}	0.0477	0.0164

TABLE II. Second level derived products, derived ratios. (These values were derived from the images in Fig. 6.)

	40 m	60 m
R_{scalar}	5.9%	5.0%
R_{vector}	3.49%	2.13%
μ_d	0.744	0.441
μ_u	0.788	0.332

TABLE III. Third level derived products, 40 to 60 m. (These values were derived from the images in Fig. 6.)

K_{Ed}	0.043 m^{-1}
K_{Eu}	0.067 m^{-1}
K_{Eod}	0.045 m^{-1}
K_{Eou}	0.053 m^{-1}
a	0.030 m^{-1}
K/a	1.50
b	0.09 m^{-1}
$c_{calculated}$	0.12 m^{-1}
$c_{measured}$	0.12 m^{-1}

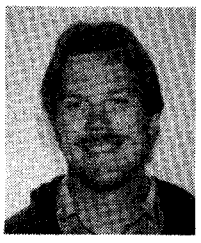

Kenneth J. Voss received the BS degree from Washington State University, Pullman, in 1979 and the Ph.D. degree from Texas A&M University, College Station, in 1984, both in physics. Since then he has been a researcher at Scripps Institution of Oceanography, first at the Visibility Laboratory and then at the Institute of Marine Resources. His research interests include ocean optics, light scattering, radiative transfer, and underwater imaging. Dr. Voss is a member of the American Geophysical Union, the Optical Society of America, and SPIE.